

Dibenzo[*b,f*]phosphepines: Novel Phosphane–Olefin Ligands for Transition Metals

Volodymyr Lyaskovskyy,^{†,‡} Relinde J. A. van Dijk-Moes,[†] Sebastian Burck,[†] Wojciech I. Dzik,[‡] Martin Lutz,[§] Andreas W. Ehlers,[†] J. Chris Slootweg,[†] Bas de Bruin,^{*,‡} and Koop Lammertsma^{*,†}

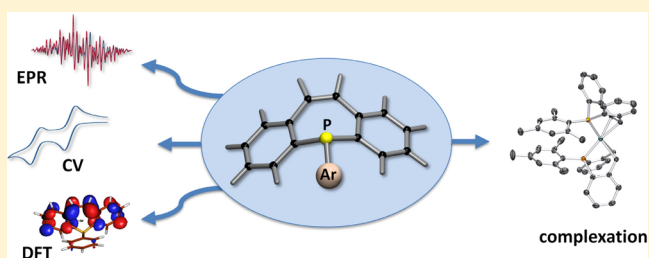
[†]Department of Chemistry and Pharmaceutical Sciences, VU University Amsterdam, De Boelelaan 1083, 1081 HV Amsterdam, The Netherlands

[‡]Van 't Hoff Institute for Molecular Sciences (HIMS), Homogeneous and Supramolecular Catalysis, University of Amsterdam (UvA), Science Park 904, 1098 XH Amsterdam, The Netherlands

[§]Crystal and Structural Chemistry, Bijvoet Center for Biomolecular Research, Utrecht University, Padualaan 8, 3584 CH Utrecht, The Netherlands

Supporting Information

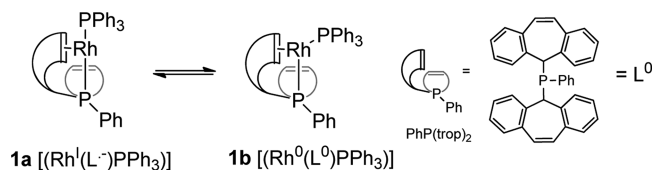
ABSTRACT: New, stable heterobidentate phosphane–olefin ligands based on the dibenzo[*b,f*]phosphepine backbone are reported together with their redox properties and coordination chemistry to rhodium(I). The X-ray crystal structures and DFT calculations show different conformations for the *P*-phenyl (**6a**) and *P*-mesityl (**6b**) derivatives. Cyclic voltammetry (vs Fc/Fc⁺) of **6a** supported by UV–vis spectroelectrochemistry showed two cathodic waves, a reversible one at $E_{1/2} = -2.62$ V ($I_f/I_b = 1.0$) and a quasi-reversible ($I_f/I_b \approx 1.2$) one at $E_{1/2} = -3.03$ V. Reduction with sodium afforded a mixture of the radical anion [**6a**]^{•−}, characterized by EPR spectroscopy, and dianion [**6a**]^{2−}, for which an X-ray crystal structure was obtained. Both **6a** and **6b** bind to Rh^I centers, giving rise to 3:1 (**8a**) and 2:1 (**8b**) ligand:Rh complexes, respectively. Two dibenzo[*b,f*]phosphepines in **8a** and **8b** act as heterobidentate ligands in which both the phosphorus atom and the olefinic double bond coordinate to rhodium, but the third ligand in **8a** binds as a monodentate P-donor. The cyclic voltammogram of **8b** showed two close-lying waves, a one-electron reversible wave at -1.45 V and a two-electron quasi-reversible wave at -1.80 V ($I_f/I_b \approx 1.3$). **8a** showed a reversible wave at -1.71 V and irreversible waves at lower potentials.



INTRODUCTION

Olefin complexes of transition metals, while known for almost 200 years, remain of immense importance.¹ They are crucial intermediates in alkene modifications, where coordination of the double bond to the metal center is the first step in the catalytic transformation, as exemplified in the oxidation at palladium (Wacker oxidation), the reduction at rhodium (Wilkinson's catalyst), and various hydrofunctionalizations (hydroamination, hydroformylation, hydrocyanation, etc.).² As auxiliary ligands, olefins steer transition-metal-catalyzed 1,4-additions and (transfer) hydrogenations.^{3,4} Especially valuable are heterobidentate ligands that contain, in addition to the olefin, an amine or phosphane donor group.⁵ Recently, a tridentate PhP(trop)₂ ligand (Scheme 1) was shown to form two unprecedented electromeric complexes with rhodium that differ substantially in their electronic structure (one isomer is the metal-centered radical [Rh⁰(L⁰)PPh₃] (**1b**) while the other is the ligand-centered radical [Rh^I(L^{•−})PPh₃] (**1a**)) but only slightly in their conformation.⁶ Phosphane–olefin ligands have further shown potential as “hydrogen reservoirs” in hydrogenation catalysis, wherein the olefin part of the ligand gets reversibly hydrogenated under the catalytic conditions, which

Scheme 1. Electromeric Phosphane–Olefin Complexes

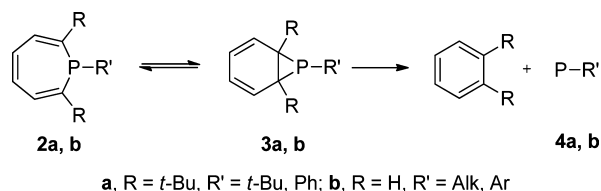


allows hydrogen transfer to the substrate via the “cooperative ligand”. This behavior potentially leads to faster reactions and special selectivities.^{4,7}

The noted examples point to intriguing properties associated with heterobidentate phosphane–olefin ligands and thereby call for new ones to apply in homogeneous catalysis and potentially expand the scope of electromers. Hence, we targeted the synthesis of phosphepines **2**, which differ from the known PhP(trop)₂ framework in that the phosphorus atom is embedded in the seven-membered ring (Scheme 2). The coordination chemistry of **2** is virtually unknown. We are aware

Received: October 30, 2012

Scheme 2. Decomposition Pathway of Phosphpepines



of only a single bidentate complex with iridium⁸ and a few monodentate P-coordination complexes.⁹ The underlying reason is the thermal lability of the phosphpepine. So far, only the parent di-*tert*-butyl phosphpepine **2a** has been isolated and characterized.¹⁰ Less crowded phosphpepines (**2b**) are elusive, since they cyclize to unstable phosphanorcaradienes (**3b**) that eliminate phosphinidenes (**4b**).¹¹ The stability of phosphpepines improves significantly on benzannulation,¹² as is the case for dibenzophosphpepines **6** (Scheme 3).¹³ Here we report on their synthesis, conformational analysis, (spectro)electrochemical behavior, and coordination chemistry to rhodium(I).

RESULTS AND DISCUSSION

Synthesis. Dibenzo[*b,f*]phosphpepines **6a** (R = Ph) and **6b** (R = Mes) were synthesized quantitatively, as monitored by ³¹P NMR spectroscopy, from (*Z*)-dibromostilbene **5** by lithiation with *tert*-butyllithium and addition of the corresponding aryldichlorophosphane at -78 °C (Scheme 3) but proved difficult to isolate due to oxidation of the phosphorus atom during chromatography.¹⁴ Therefore, BH₃-SMe₂ was added to obtain the readily purifiable borane complexes (yields 82% (**7a**), 32% (**7b**); ³¹P NMR 13.4 ppm (**7a**), 10.4 ppm (**7b**)), which on deprotection with DABCO (16 h, room temperature, DCM or toluene as solvent) afforded the desired dibenzo[*b,f*]phosphpepines **6** (yields 97% (**6a**), 96% (**6b**); ³¹P NMR -8.1 ppm (**6a**), -30.5 ppm (**6b**)).

Crystals suitable for X-ray diffraction were obtained by slow vapor diffusion of pentane into dichloromethane solutions of **6a,b**. Both molecular structures (Figure 1) have P–C bond lengths similar to those in triarylphosphanes (1.82–1.84 Å for **6a** and **6b** vs 1.83 Å for PPh₃).¹⁵ The sum of the bond angles around phosphorus reveals comparable pyramidalities for **6a** (308.96(10)°) and **6b** (312.21(15)°), as for PPh₃ (309°), but the conformations differ. The phenyl group of **6a** is oriented parallel to the heterocyclic double bond and has an acute dihedral angle of 60.98(9)° with the phosphpepine P1–C1–C14 plane, thereby rendering the phosphorus lone pair in the same spatial direction as the benzannulated rings (Figure 1, left). The molecular structure of **6b** is quite different, with its mesityl

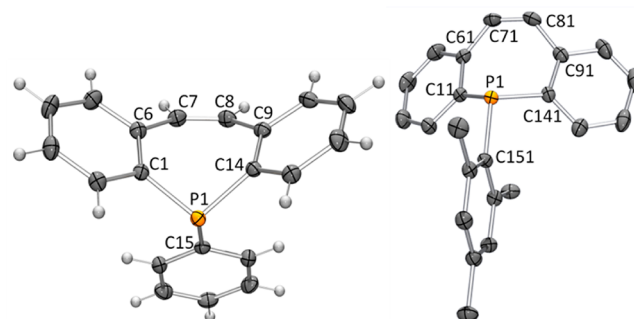


Figure 1. Molecular structures of **6a** (left) and **6b** (right) in the crystal form. Displacement ellipsoids are drawn at the 50% probability level. Selected bond lengths (Å), bond angles (deg), and torsion angles (deg) are as follows. **6a**: P1–C1 = 1.8247(13), P1–C15 = 1.8373(13), C1–C6 = 1.4089(18), C7–C8 = 1.338(2), C6–C7 = 1.4669(19); C1–P1–C15 = 102.42(6), C1–P1–C14 = 102.84(6), C15–P1–C14 = 103.70(6); C16–C15–P1–C14 = 38.01(12). **6b** (only one of two independent molecules is shown; hydrogen atoms are omitted for clarity): P1–C11 = 1.8348(19), P1–C151 = 1.840(2), C11–C61 = 1.411(2), C71–C81 = 1.332(3), C61–C71 = 1.468(3); C11–P1–C151 = 102.60(9), C11–P1–C141 = 105.16(8), C151–P1–C141 = 104.45(9); C161–C151–P1–C141 = $-52.94(18)$.

group almost perpendicular to the phosphpepine ring and the phosphorus lone pair oriented in the direction to the vinylic bond instead of the benzannulated rings (Figure 1, right). Hence, **6b** is preorganized to bind transition metals in a heterobidentate manner, while **6a** has to undergo pyramidal inversion at phosphorus to bind metals in a similar manner.

The flexibility of the two dibenzo[*b,f*]phosphpepines was investigated computationally at the B3PW91/6-311G(d,p) level of theory.¹⁶ Three different conformations I–III were identified for **6a** and **6b** each (Figure 2; **6b**' lacks the mesityl's

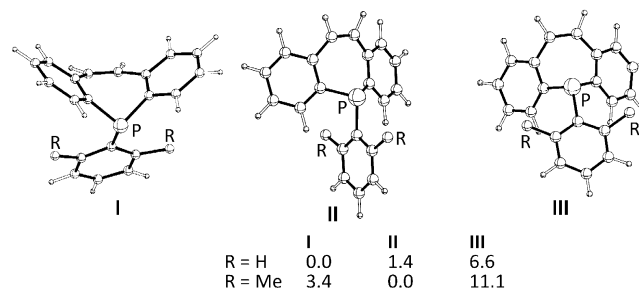
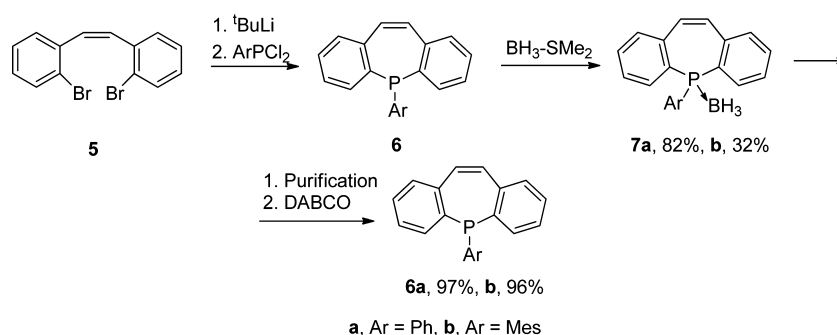


Figure 2. Conformations of *P*-aryl dibenzo[*b,f*]phosphpepines and their relative B3PW91/6-311G(d,p) energies (in kcal mol⁻¹, ZPE corrected).

Scheme 3. Synthesis of the Dibenzo[*b,f*]phosphpepines **6a** and **6b** from (*Z*)-Dibromostilbene **5**

p-CH₃ group for simplicity). **I** resembles the molecular structure of **6a** and **II** that of **6b**, while the aryl group in **III** is rotated by 90° around the P–C bond as compared to the case for **II**. In agreement with the experimentally obtained crystal structures, **I** is energetically favored for the phenyl derivative **6a** over **II** and **III** by 1.4 and 6.6 kcal mol⁻¹, respectively, and **II** is favored for **6b'** over **I** and **III** by +3.4 and +11.1 kcal mol⁻¹, respectively. It is evident that the *o*-methyl groups of the *P*-aryl substituent have a significant impact on the conformational stability of the dibenzo[*b,f*]phosphepine.

While the experimentally observed conformational difference between **6a** and **6b** in the solid state are in agreement with the above DFT conformational analysis, we cannot exclude an additional influence of the crystal packing. In the crystal structure of **6b** π – π interactions between the mesityl ring of one molecule and the aryl ring of the dibenzophosphepine moiety of another molecule are apparent (see Supporting Information, Figure S9).

The NMR (both ³¹P and ¹H) spectra of **6a** and **6b** do not reveal the presence of different conformers, indicating a rapid equilibrium between the two major conformers **I** and **II** on the NMR time scale for both **6a** and **6b** (the third isomer **III** seems to be too high in energy to contribute significantly), which is in agreement with the low calculated barrier for **I** → **II** interconversion (~6 kcal mol⁻¹) in structurally related phosphepine systems.^{11a}

Cyclic Voltammetry and UV–Vis Spectroelectrochemistry. To investigate the electron-accepting properties of the dibenzo[*b,f*]phosphepine ligands, we investigated the redox behavior of **6a** with cyclic voltammetry (CV). In THF **6a** shows no redox activity in the potential range between –2.45 and +0.50 V (vs Fc/Fc⁺, Figure 3). At +0.55 V there is an onset of

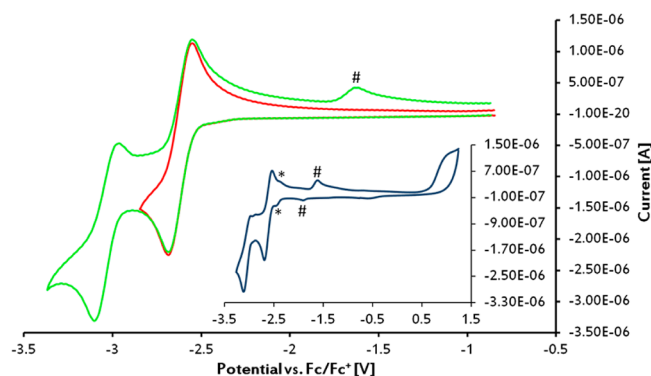
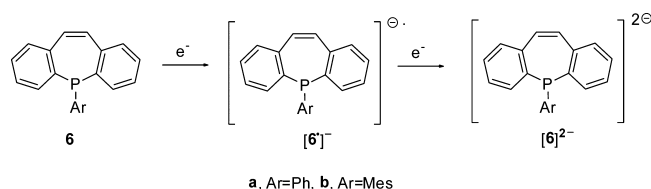


Figure 3. Cyclic voltammograms of **6a**: full (blue) and separate (red) scans over the first reduction wave and full (green) scan over the second one. Scan rate: 200 mV s⁻¹. Signals marked with * stem from the irreversible oxidation at potentials >+0.55 V. Signals marked with # are attributed to a reaction product of [6a]²⁻ with traces of water (see text).

an irreversible oxidation. The CV shows a reversible cathodic wave at $E_{1/2} = -2.62$ V that forms the dibenzophosphepine radical anion [6a]^{•-} (Scheme 4). A second wave, corresponding to the transfer of a second electron to form the phosphepine dianion [6a]²⁻, appears at $E_{1/2} = -3.03$ V. Measurements in commonly purified solvents and electrolyte first indicated that this wave is not fully reversible; scanning over it resulted in the appearance of a followup product showing an anodic wave at –1.76 V (marked with # in Figure 3). The two-electron-reduced phosphepine apparently reacts

Scheme 4. One- and Two-Electron Reduction of Dibenzo[*b,f*]phosphepine **6**



even with traces of water in the solvent/electrolyte, leading to the redox active followup product observed with CV. More rigorous exclusion of water resulted in a fully reversible wave at –2.62 V.

We conclude that the accessibility and reversibility of both reduction waves are indicative of the electron-accepting ability of **6a**, suggesting that dibenzo[*b,f*]phosphepines can indeed be suitable π -acceptors and/or redox-noninnocent ligands in coordination chemistry.^{17,18}

The electrochemical reduction of benzophosphepines **6a** in THF was also monitored by UV–vis spectroelectrochemistry using an optically transparent thin-layer electrochemical (OTTLE) cell. The spectrum shows an absorption at 304 nm (in addition to strong ones below 280 nm), which upon one-electron reduction gradually disappears with new absorptions emerging at 322, 350, 508, and 831 nm (Figure 4, left). On the basis of TD-B3LYP/def2-TZVP calculations,¹⁹ most of these bands can be assigned to stem from transitions from the SOMO to higher lying orbitals (see Table 1).

The three characteristic absorptions of [6a]^{•-} disappear in the second reduction step when a single new absorption emerges at 552 nm. This corresponds to filling the SOMO of [6a]^{•-} with an additional electron and limits the possible optical transitions for the diamagnetic, closed-shell [6a]²⁻. Its TD-DFT calculated spectrum gives three absorptions at 416, 505, and 628 nm, of which the blue-shifted absorption is of very low intensity. A similar weak absorption at 405 nm is observed in the experimental spectrum. The calculated strong absorption at 505 nm and the weak absorption at 628 nm are interpreted to jointly correlate with the observed broad absorption at 552 nm (see Table 1). Additional weak absorptions are predicted by the TD-DFT calculations at 1051 nm for [6a]^{•-} and 889 nm for [6a]²⁻, but these are not observed in the experimental spectra (probably due to their weakness and broadening). The TD-DFT calculations do not reproduce the experimental electronic spectra very precisely, and some deviations in the range between 400 and 700 nm are apparent. The calculated band at 423 nm for [6a]^{•-} is predicted at an overly high energy (experimental 508 nm), while for [6a]²⁻ the predicted energy separation between the two calculated bands at 628 and 505 nm is larger than that observed (one broad peak at 508 nm). Nonetheless, overall the calculations provide a useful guideline to assign the bands.

Chemical Reduction of the Dibenzophosphepines with Elemental Sodium. Encouraged by the CV and UV–vis spectroelectrochemical results, we set out to synthesize and isolate the singly (1e) and hopefully the doubly (2e) reduced dibenzo[*b,f*]phosphepines. On the basis of the CV data we chose elemental sodium as a reducing agent ($E^\circ(\text{Na}) = -3.04$ V vs Fc/Fc⁺).²⁰ When 10 equiv was added at room temperature to a solution of **6a** in THF, the initial yellow mixture turned deeply purple over 4 h. The EPR spectrum confirmed that the

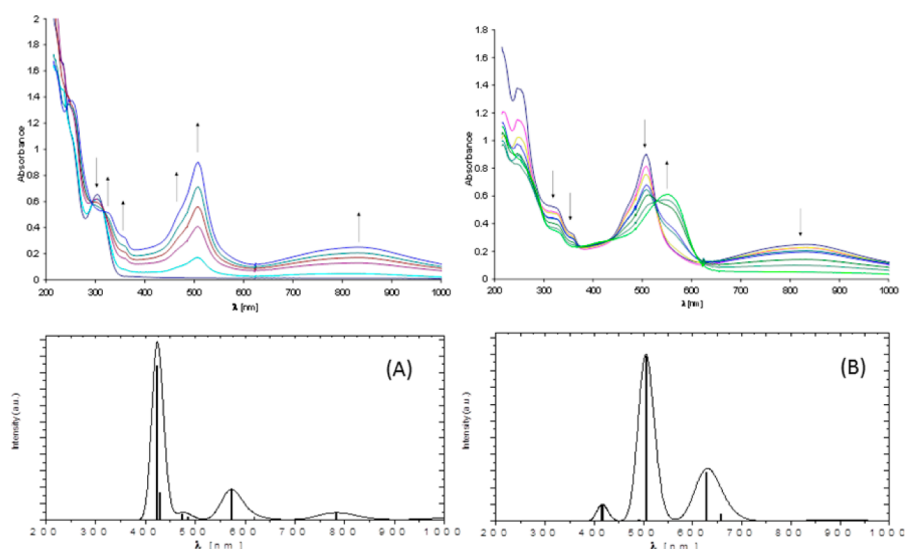


Figure 4. (top) Evolution of the UV–vis spectra during the first (left) and second (right) reductions of **6a**. (bottom) Calculated (Orca) TD-DFT, B3LYP/def2-TZVP spectra (lowest 10 transitions in the visible range) of $[\mathbf{6a}^{\bullet-}]$ (A) and $[\mathbf{6a}]^{2-}$ (B).

Table 1. TD-DFT Parameters of the UV–Vis Spectra of $[\mathbf{6a}^{\bullet-}]$ and $[\mathbf{6a}]^{2-}$

compd	λ_{exptl}^b nm	λ_{calcd}^a nm	rel intensity, % ^{aa}	main excitation
$[\mathbf{6a}^{\bullet-}]$	831	1051	2	SOMO → LUMO+3
	tail	783	5	SOMO → LUMO+4
	508	618	2	SOMO → LUMO+5
	~480 (sh)	572	20	SOMO → LUMO+6
	466	485	2	SOMO → LUMO+7
	tail	473	4	HOMO → SOMO
	350, 322	429	18	SOMO → LUMO+9
$[\mathbf{6a}]^{2-}$	350, 322	423	100	HOMO → SOMO
	552	889	1	SOMO → LUMO+3
		628	30	HOMO → LUMO+5
		505	100	HOMO → LUMO+6
	405	416	10	HOMO → LUMO+6

^aOrca, TD-DFT, B3LYP/def2-TZVP, COSMO $\epsilon = 2.28$.

radical anion $\text{Na}^+[\mathbf{6a}^{\bullet-}]$ had formed (Figure 5a, Scheme 4); the solution was NMR silent.

A satisfactory EPR spectrum could be simulated with parameters that reflect delocalization of the spin density over the olefinic and aromatic carbons (Table 2, Figure 5). Resolved hyperfine couplings with 13 nuclei in 7 independent sets were obtained: i.e., with the phosphorus atom, the olefinic hydrogens (H1), four sets of aromatic hydrogen nuclei (H2–5), and a small, poorly resolved coupling with the meta hydrogens (H7) of the phenyl substituent (Figure 5a). The assignment of the hyperfine couplings is based on supporting DFT calculations (ORCA, B3LYP/TZVP,¹⁹ geometry optimized with Turbomole at the BP86/SV(P) level²¹) of $\text{Na}^+[\mathbf{6a}^{\bullet-}]$ (Table 2, Supporting Information). Evidently, reducing **6a** to $[\mathbf{6a}^{\bullet-}]$ places an electron in the fully delocalized π^* SOMO with a similarly shaped spin density distribution (Figure 6) in support of the observed EPR spectrum.

The EPR spectrum for the mesityl-derivative $\text{Na}^+[\mathbf{6b}^{\bullet-}]$ was obtained likewise (Figure 5b), but it is broader than that of $\text{Na}^+[\mathbf{6a}^{\bullet-}]$ even at low concentrations. Consequently, the

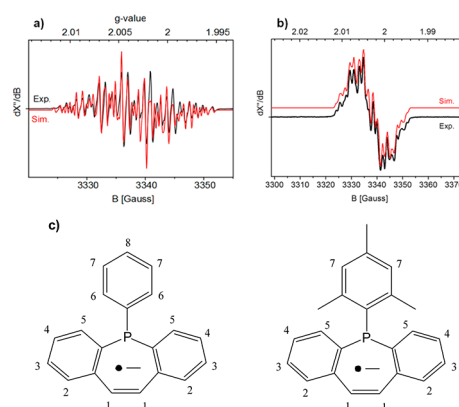


Figure 5. Experimental (in THF) and simulated EPR spectra of (a) $\text{Na}^+[\mathbf{6a}^{\bullet-}]$ (frequency 9.357723 GHz; microwave power 2 mW; $T = 298$ K; modulation amplitude 1 G) and (b) $\text{Na}^+[\mathbf{6b}^{\bullet-}]$ (frequency 9.359971 GHz; microwave power 2 mW; $T = 298$ K; modulation amplitude 0.2 G). (c) Atom numbering used for the hyperfine couplings in Table 2.

Table 2. Experimental and DFT g Values and Hyperfine Couplings (MHz) of $\text{Na}^+[\mathbf{6a}^{\bullet-}]$ and $\text{Na}^+[\mathbf{6b}^{\bullet-}]$

	$[\mathbf{6a}^{\bullet-}]$		$[\mathbf{6b}^{\bullet-}]$	
	exptl ^a	DFT ^b	exptl ^a	DFT ^b
g_{iso}	2.0034	2.0027	2.0030	2.0024
hyperfine coupling ^c				
P	−11.34	−12.93	−16.3	−13.5
H1 ^d	−10.74	−12.41	−11.1	−12.3
H2 ^d	−6.10	−7.40	−4.0	−6.6
H3 ^d	3.01	2.56	3.8	2.1
H4 ^d	−8.20	−11.83	−9.4	−11.1
H5 ^d	4.49	4.42	2.0 ^e	4.7
H7 ^d	−0.36 ^e	−0.54	not resolved	−0.02, 0.04

^aDerived from least-squares curve fitting of the spectrum recorded in THF at $T = 298$ K. The signs were assigned on the basis of the DFT calculations. ^bB3LYP/TZVP. ^cSee Figure 5 for atom numbering. ^dTwo equivalent hydrogens. ^ePoorly resolved.

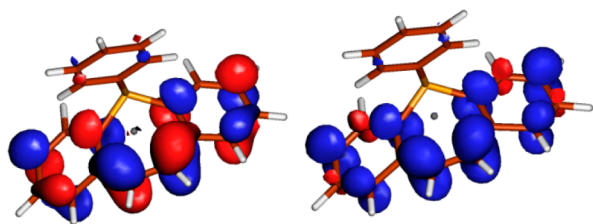


Figure 6. SOMO (left) and spin density (right) distribution of $[6a^{\bullet}]^{-}$.

smallest hyperfine couplings with the H5 hydrogens are poorly resolved and those with the H7 hydrogens of the *P*-Mes group are not resolved at all (Figure S5b, Table 2). The spectrum could be simulated in a satisfactory manner using the DFT-calculated values for $[6b^{\bullet}]^{-}$ as a starting point (Table 2, Supporting Information). The DFT optimized structures of the two radical anions adopt the same conformations as their neutral precursors, that is **I** for $[6a^{\bullet}]^{-}$ and **II** for $[6b^{\bullet}]^{-}$ (Figure 2), but with longer C7–C8 double (1.39–1.40 Å vs 1.35 Å) and shorter C6–C8 single bonds (1.42 vs 1.46 Å) for the seven-membered ring, reflecting its delocalized nature (see Figure 1 for numbering).

Single crystals suitable for X-ray diffraction were obtained by slow vapor diffusion of pentane into the THF solution obtained from the reaction of **6a** with sodium. Surprisingly, these proved to be of dianionic $[Na^+]_2[6a]^{2-}$ (Figure 7) instead of the expected radical anion $[Na^+][6a^{\bullet}]^{-}$, which was observed by EPR spectroscopy. Dianion $[6a]^{2-}$ crystallizes as a dimer with two $[6a]^{2-}$ species bridged by three THF molecules ($[Na^+]_4[6a^{2-}]_2 \cdot 7THF$) (Figure 7). Apparently, the purple solution that is obtained by mixing **6a** with 10 equiv of

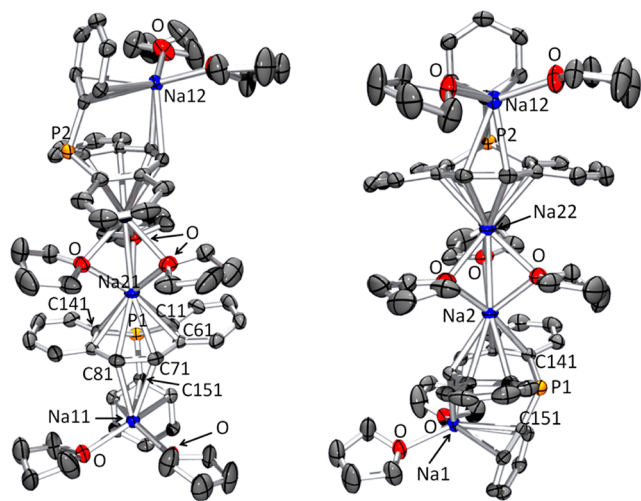


Figure 7. Molecular structure of $[Na^+]_4[6a^{2-}]_2 \cdot 7THF$ (two different viewpoints are shown for clarity) from an X-ray crystal structure determination (hydrogen atoms and disordered noncoordinated solvent molecules are omitted for clarity, only major disorder components of the THF molecules are shown). Displacement ellipsoids are drawn at the 50% probability level. Selected bond lengths (Å), bond angles (deg), and torsion angles (deg): P1–C11 = 1.811(2), P1–C151 = 1.8524(18), C11–C61 = 1.462(3), C71–C81 = 1.462(3), C61–C71 = 1.396(3), Na1–C71 = 2.7515(19), Na1–C81 = 2.592(2), Na1–C151 = 2.7494(18), Na1–C161 = 2.8596(19), Na2–C71 = 2.6818(19), Na2–C81 = 2.6707(19); C11–P1–C151 = 100.60(8), C11–P1–C141 = 110.27(9), C151–P1–C141 = 99.94(8); C161–C151–P1–C141 = 45.46(15).

metallic sodium consists of a mixture containing both the singly and doubly reduced products $[Na^+][6a^{\bullet}]^{-}$ and $[Na^+]_2[6a]^{2-}$.

The molecular structure of the dianion adopts conformation **I** just like the neutral precursor, but charge delocalization profoundly effects the C–C bonds, lengthening the “aromatic” C1–C6 ($[6a]^{2-}$ 1.462(3) Å vs **6a** 1.4089(18) Å) and C7–C8 “double” bonds ($[6a]^{2-}$ 1.462(3) Å vs **6a** 1.338(2) Å) and shortening the C6–C7 “single” bonds ($[6a]^{2-}$ 1.396(3) Å vs **6a** 1.4669(19) Å), while the P-pyramidalty remains essentially unchanged (sum of the bond angles around phosphorus: $[6a]^{2-}$ 310.81(14)° vs **6a** 308.96(10)°).

Magnetic susceptibility measurements at room temperature on crystals of $[6a]^{2-}$ ($\mu_{\text{eff}} \approx 0$) support a closed-shell configuration, which is favored by 14.9 kcal mol^{−1} over the triplet excited state according to B3LYP/6-311(d,p) calculations. Nonetheless, no ³¹P NMR spectrum of diamagnetic $[6a]^{2-}$ could be recorded, likely due to the presence of (trace amounts of) the radical anion, as rapid electron transfer between the two species is expected to cause substantial NMR signal broadening.

Two mechanistic pathways can lead to formation of dianion $[6a]^{2-}$. First, reduction of $[6a^{\bullet}]^{-}$ with excess sodium may occur. The redox potential corresponding to the second reduction of **6a** ($E_{1/2} = -3.03$ V vs Fc/Fc⁺) is very close to the reduction potential of sodium ($E^{\circ} = -3.03$ V vs Fc/Fc⁺), which does in fact explain the presence of both $[6a^{\bullet}]^{-}$ and $[6a]^{2-}$ in the reaction mixture.²⁰ Second, disproportionation ($2[6a^{\bullet}]^{-} \rightleftharpoons [6a]^{2-} + 6a$) may be followed by selective crystallization of $[Na^+]_2[6a]^{2-}$. On the basis of the CV redox potentials, this disproportionation equilibrium lies strongly to the left ($\Delta G^{\circ} = 9.4$ kcal mol^{−1}), but crystallization of $[6a]^{2-}$ may be feasible given the equilibrium constant of $K_{\text{disp}} \approx 1 \times 10^{-7}$.

Unfortunately, we were unable to grow crystals of $[Na^+]_2[6b]^{2-}$, possibly due to its higher solubility. However, like its neutral precursor, B3PW91/6-311G(d,p) calculations show a preference for conformation **II** and, like $[6a]^{2-}$, elongated “aromatic” and “double” C–C bonds ($d_{C7-C8} = 1.35$ (**6b'**), 1.42 Å ($[6b']^{2-}$); $d_{C1-C6} = 1.41$ (**6b'**), 1.46 Å ($[6b']^{2-}$)) and shortened “single” bonds ($d_{C6-C7} = 1.46$ (**6b'**), 1.40 Å ($[6b']^{2-}$)) for the phosphepine ring.

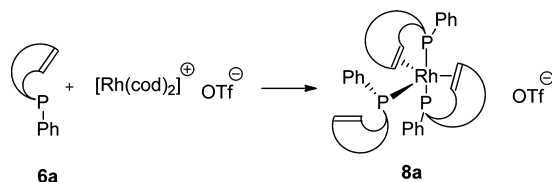
In summary, the collective UV–vis, structural, and computational data show that upon 1e reduction an electron is placed in the π^* LUMO of **6**, being the SOMO of $[6^{\bullet}]^{-}$, and two on 2e reduction, forming the HOMO of $[6]^{2-}$ without changing the conformation, which is **I** for the *P*-phenyl and **II** for the *P*-mesityl derivative (Figures 6 and Figures S6 and S8 (Supporting Information)). Electronically, the dibenzo[*b,f*]phosphepines in $[6^{\bullet}]^{-}$ and $[6]^{2-}$ are then best viewed as a combination of two isolated fragments, namely a 1e- or 2e-reduced π -conjugated stilbene part and a noninteracting phosphane lone pair, making them ideal ligands for coordination chemistry.

Complexation to Rhodium(I). To probe the ability of **6a** and **6b** to act as heterobidentate phosphane–olefin ligands, we investigated their affinity for Rh^I precursors as a necessary first step toward exploring their “redox noninnocence” features and behavior in catalysis. First, we show that both are potent chelating ligands, despite their conformational differences.

We start with the coordination chemistry of ligand **6a**. Despite the fact that the phosphorus lone pair and the olefinic double bond of the free ligand are not preorganized for metal chelation (Figure 2), pyramidal inversion at P1 occurs readily, allowing the ligand to act as a heterobidentate phosphane–

olefin ligand. The reaction of **6a** with $[\text{Rh}(\text{cod})_2][\text{OTf}]$ in a 3:1 ratio in DCM (room temperature, 16 h) led to the quantitative formation of the yellow tris-coordinated complex **8a** (Scheme 5). A lower ligand: Rh ratio (2:1) also leads to formation of **8a** (based on ^{31}P NMR), but with incomplete conversion of the Rh^{I} precursor.

Scheme 5. Coordination of **6a** with Rh^{I} Species



The molecular structure of **8a**, resolved by X-ray crystal structure determination (Figure 8), reveals a strongly distorted

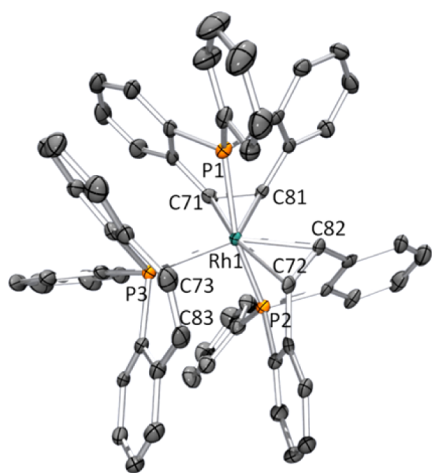


Figure 8. Molecular structure of the cationic Rh complex **8a** in the crystal (hydrogen atoms, disordered solvent molecules, and the triflate counterion are omitted for clarity). Only one of the two independent molecules is shown. Displacement ellipsoids are drawn at the 50% probability level. Selected bond lengths (Å) and angles (deg): P1–Rh1 = 2.3667(11), P2–Rh1 = 2.2973(11), P3–Rh1 = 2.4232(11), C71–C81 = 1.432(6), C72–C82 = 1.422(6), C73–C83 = 1.334(6), C61–C71 = 1.492(6), $\text{Rh1}-\frac{1}{2}(\text{C71}-\text{C81}) = 2.076(3)$, $\text{Rh1}-\frac{1}{2}(\text{C72}-\text{C82}) = 2.110(3)$; P1–Rh1–P3 = 95.29(4), P1–Rh1–P2 = 164.47(4), $\frac{1}{2}(\text{C71}-\text{C81})-\text{Rh1}-\frac{1}{2}(\text{C72}-\text{C82}) = 127.72(12)$.

trigonal bipyramidal complex ($\tau = 0.61$)²² carrying two heterobidentate benzophosphepine ligands with axial phosphorus atoms and equatorial double bonds and a third (equatorial) benzophosphepine that coordinates to the rhodium by its phosphorus atom only. This Rh–P3 bond is longer than the other Rh–P1 and Rh–P2 bonds (2.4232(11) vs 2.2973(11)–2.3667(11) Å). Rh coordination substantially elongates the olefinic bonds (1.422(6)–1.432(6) vs 1.334(6) Å), which points to substantial π -back bonding and hence a strong metallo-cyclopropane resonance contribution. Remarkably, complex **8a** adopts conformations **II** and **III** for the bidentate ligand and **II** for the monodentate ligand, in contrast to the preferred conformation **I** for the free ligand (Figure 2). This may be of steric origin, although chelating effects may also contribute.

The room-temperature ^{31}P NMR spectrum of **8a** shows a sharp doublet of triplets ($^1J_{\text{PRh}} = 119.0$, $^2J_{\text{PP}} = 29.5$ Hz) at 20.5

ppm and a very broad signal at 36.0 ppm (Figure 9a). Lowering the temperature leads to sharpening of the low-field signal to three doublet of doublets of doublets at 215 K (^{31}P NMR 19.7 ppm ($^1J_{\text{PRh}} = 119.0$, $^2J_{\text{PP}} = 38.1$, $^3J_{\text{PP}} = 21.8$ Hz), 31.4 ppm ($^2J_{\text{PP}} = 395.0$, $^1J_{\text{PRh}} = 95.2$, $^2J_{\text{PP}} = 21.8$ Hz), 39.2 ppm ($^2J_{\text{PP}} = 395.0$, $^1J_{\text{PRh}} = 95.2$, $^2J_{\text{PP}} = 38.1$ Hz)) (Figure 9f). The signals at 39.2 and 31.4 ppm show a very large *trans* $^2J_{\text{PP}}$ coupling constant of 395.0 Hz and are therefore assigned to stem from the two *trans*-positioned phosphorus atoms in the bipyramid.

VT- ^{31}P NMR (Figure 9) reveals a dynamic process due to Rh–P3 bond rotation of the monodentate ligand in **8a** (Scheme 6). The magnetic anisotropy of the aryl rings of this ligand affects the chemical shifts of the two *trans*-positioned axial phosphorus atoms, which explains their inequivalence (39.2 and 31.4 ppm) below the coalescence temperature and their dynamic interconversion above. Rotation of the monodentate ligand does not affect its own chemical shift in the 215–298 K temperature range but averages the $^2J_{\text{PP}}$ couplings with the axial P atoms ($^2J_{\text{PP}} = 38.1$ and 21.8 Hz) to $^2J_{\text{PP}} = 29.5$ Hz at the coalescence temperature, where these atoms become equivalent on the NMR time scale. The experimental ΔG^\ddagger value for Rh–P3 bond rotation of the equatorial ligand is estimated at 12.6 kcal mol^{−1}.²³

In sharp contrast to the Rh^{I} coordination of **6a**, the analogous reaction with **6b** yielded (91%) by ^{31}P NMR a 10:1 mixture of the square-planar $[\text{Rh}(\text{6b})_2][\text{OTf}]$ complexes *cis*-**8b** ($\delta(^{31}\text{P})$ 34.6 ppm, $^1J_{\text{PRh}} = 149.0$ Hz) and *trans*-**8b** ($\delta(^{31}\text{P})$ 43.1 ppm, $^1J_{\text{PRh}} = 127.3$ Hz), which carry two instead of three ligands (Scheme 7). It is noteworthy that **8b**, in contrast to **8a**, does not reveal any dynamic behavior on the NMR time scale. Deep red crystals of the major isomer *cis*-**8b** were obtained in 55% yield by slow evaporation of pentane into the dichloromethane solution of the mixture. The molecular structure of **8b** (Figure 10) reveals a *cis* coordination mode for the two dibenzophosphepine rings. In the crystal structure we find an intramolecular π -stacking interaction between the two mesityl substituents. These substituents are nearly parallel (deviation 2.62(11) $^\circ$), and the centers of the rings have perpendicular distances to the neighboring ring plane of 3.5945(9) and 3.5807(11) Å, respectively. This interaction may explain the relative stability of *cis*-**8b** over the *trans*-**8b** isomer. Dibenzophosphepine in *cis*-**8b** adopts conformation **III**, which is higher in energy than conformation **II** for the free ligand. Coordination of this higher energy conformation is perhaps less surprising than is the case for **8a**. Obviously, **II** would lead to substantial steric repulsion between two mesityl rings in *cis*-**8b**.

The phosphorus atoms of **8b** (320.74(16) $^\circ$ for P1 and 320.14(17) $^\circ$ for P2) are slightly less pyramidal than in **6b** (312.21(15) $^\circ$) and dianion $[\text{6a}]^{2-}$ (310.81(14) $^\circ$) according to the sums of their bond angles. The P–Rh bonds have lengths similar to the equatorial bonds of **8a** (2.2823(5)–2.3079(5) vs 2.2973(11)–2.3667(11) Å), and the C7–C8 double bonds are likewise elongated compared to those of the free ligand (1.400(3)–1.405(3) vs 1.332(3)–1.339(3) Å), indicating substantial metal-to-ligand π -back-bonding. The observed difference in the ligand to Rh coordination stoichiometry between **8a** (3:1) and **8b** (2:1) is presumably caused by the steric crowding of the methyl groups in **6b**.

Complex *cis*-**8b**[OTf] is sparsely soluble in ethers, which hampers a study of its redox properties. To increase the solubility in THF, we exchanged the triflate ion by stirring *cis*-**8b**[OTf] with NaBARF (BARF[−] = B(C₆H₃(CF₃)₂)₄[−]) in DCM to obtain deep red crystalline *cis*-**8b**[BARF] (80%). Its cyclic

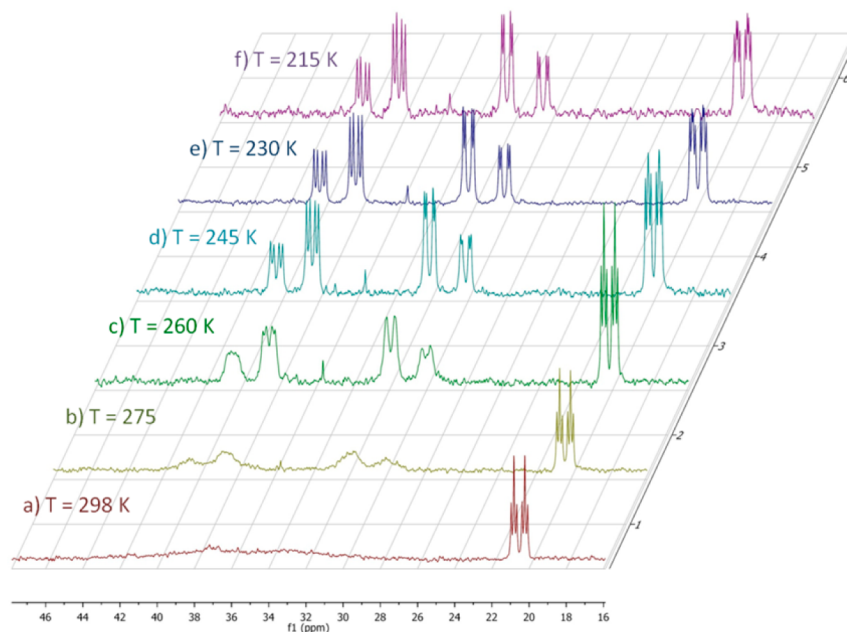
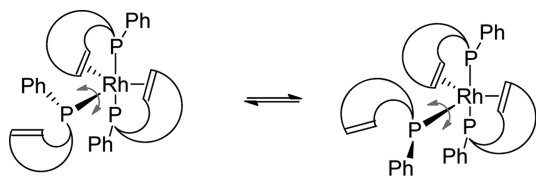
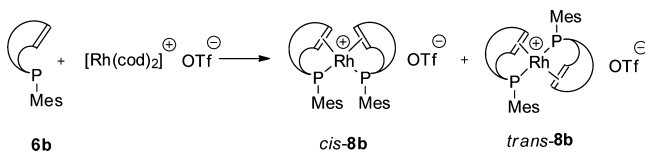


Figure 9. ^{31}P NMR spectra of the complex **8a** at different temperatures.

Scheme 6. Dynamic Behavior of Complex **8a**



Scheme 7. Coordination Chemistry of Ligand **6b** toward Rhodium(I)



voltammogram (Figure 11) shows two cathodic waves with $E_{1/2} = -1.45$ and -1.80 V (vs Fc/Fc^+). The first corresponds to a reversible one-electron reduction ($I_f/I_b = 1.0$) and the second to a nonfully reversible two-electron transfer ($I_f/I_b \approx 1.3$). Unfortunately, the closeness of these potentials and the unpreventable disproportionation hamper the isolation of the rhodium(0) radical anion,^{6,24,25} which agrees with our inability to isolate reduced species from the reaction of *cis-8b*[BARF] with either sodium or cobaltocene as reducing agent. Cyclic voltammetry of **8a** (see Supporting Information, Figure S3) revealed one reversible cathodic wave at -1.71 V and several nonreversible waves at lower potentials.

CONCLUSIONS

In this paper we describe the synthesis, redox properties, and initial coordination studies of new heterobidentate phosphane-olefin ligands based on the dibenzophosphepine scaffold. The *P*-phenyl and *P*-mesityl derivatives **6a,b** are readily synthesizable from commercially available precursors. They show interesting redox activity as free ligands and can be reduced by sodium to the radical anion [**6a** $^{\bullet-}$] and dianion [**6a** $^{2-}$],

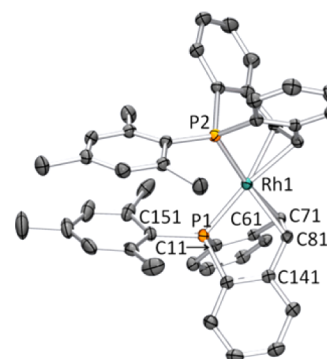


Figure 10. Molecular structure of *cis-8b* from X-ray crystal structure determination (hydrogen atoms, noncoordinated triflate counterion, and CH_2Cl_2 solvent molecules are omitted for clarity). Displacement ellipsoids are drawn at the 50% probability level. Selected bond lengths (Å), bond angles (deg), and torsion angles (deg): $\text{P1}-\text{C11} = 1.822(2)$, $\text{P1}-\text{C151} = 1.819(2)$, $\text{C71}-\text{C81} = 1.400(3)$ ($\text{C72}-\text{C82} = 1.405(3)$ in the second ligand), $\text{C61}-\text{C71} = 1.475(3)$, $\text{P1}-\text{Rh1} = 2.3079(5)$, $\text{C71}-\text{Rh1} = 2.219(2)$, $\text{C81}-\text{Rh1} = 2.201(2)$; $\text{C11}-\text{P1}-\text{C151} = 112.79(9)$, $\text{C11}-\text{P1}-\text{C141} = 94.53(9)$, $\text{C151}-\text{P1}-\text{C141} = 113.42(9)$; $\text{C161}-\text{C151}-\text{P1}-\text{C11} = -42.62(19)$.

which are electronically best described as a combination of two isolated fragments, that is a $1e$ (or $2e$) reduced stilbene fragment and a phosphane lone pair. Dibenzophosphepines deserve attention as new heterobidentate phosphane-olefin ligands in the coordination chemistry to late transition metals, as demonstrated for Rh^I. The structure of the rhodium complexes can be tuned by changing the substituents at the phosphorus atom. Thus, whereas dibenzophenyl phosphepine **6a** gives the 3:1 (ligand:Rh) complex **8a**, the more bulky mesityl analogue **6b** leads to the 2:1 complex **8b**. In the distorted-trigonal-bipyramidal **8a** two of the dibenzophosphepines act as bidentate ligands, while the third ligand binds as a monodentate P donor. In the square-planar complex *cis-8b* both dibenzophosphepine ligands **6b** coordinate in a bidentate fashion. Interestingly, the ligands in these two complexes adopt conformations that are less favorable for the noncoordinated

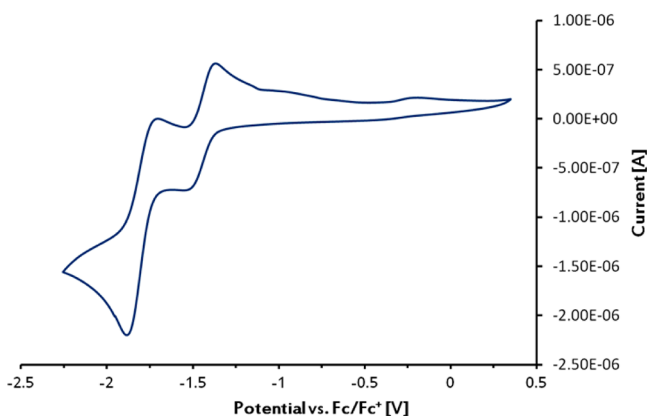


Figure 11. Cyclic voltammogram of *cis*-8b [BARF]. Scan rate: 100 mV s⁻¹.

dibenzophosphepines. These initial investigations on the dibenzophosphepine ligand system bode well for the future, where we will explore their “redox noninnocent” behavior and their potential to generate new classes of transition-metal-based catalysts.

EXPERIMENTAL SECTION

General Considerations. All syntheses were performed with the use of Schlenk techniques under an atmosphere of dry nitrogen. Pentane, THF, toluene, and diethyl ether were distilled under nitrogen from sodium; dichloromethane was distilled under nitrogen from calcium hydride. Bu₄NPF₆ was dried under vacuum.

NMR spectra were recorded at 293 K. ¹H NMR: Bruker Advance 250 (250 MHz), Bruker Advance 400 (400 MHz), Bruker UltraShield 500 (500 MHz), referenced internally to residual solvent resonance of CHCl₃ (δ 7.26 ppm) and CH₂Cl₂ (δ 5.32 ppm). ¹³C{¹H} NMR: Bruker Advance 400 (101 MHz), Bruker UltraShield 500 (126 MHz) referenced internally to residual solvent resonance of CDCl₃ (δ 77.2 ppm) and CD₂Cl₂ (δ 53.8 ppm). ³¹P{¹H} NMR: Bruker Advance 250 (101 MHz), Bruker Advance 400 (162 MHz) using 85% H₃PO₄ as an external standard (δ 0.0 ppm). ¹¹B NMR: Bruker Advance 400 (128 MHz) using BF₃·OEt₂ as an external standard (δ 0.0 ppm). ¹⁹F{¹H} NMR: Bruker Advance 250 (235 MHz) using BF₃·OEt₂ as an external standard (δ 0.0 ppm). All NMR signals are given in ppm. For numbering of the assignments see Figure S5.

IR spectra were recorded on a Bruker Alpha-P FT-IR spectrometer. Peak intensities are marked as follows: s, strong; m, medium; w, weak. All IR bands are given in cm⁻¹. High-resolution fast atom bombardment mass spectra (HR-FAB MS) were recorded on a JEOL JMS SX/SX 102A four-sector mass spectrometer, coupled to a JEOL MS-MP9021D/UPD system program. High-resolution electrospray ionization mass spectra (HR-ESI MS) were recorded on Bruker MicroTOFQ, ESI positive mode, capillary voltage 4.5 kV.

For electrochemical measurements a 2 mM phosphepine/0.1 M Bu₄NPF₆ THF solution was used. Cyclic voltammograms were recorded in a gastight single-compartment three-electrode cell equipped with platinum working (apparent surface of 0.42 mm²), coiled platinum wire auxiliary, and silver wire pseudoreference electrodes. The cell was connected to a computer-controlled PAR Model 283 potentiostat. All redox potentials are reported against the ferrocene/ferrocenium (Fc/Fc⁺) redox couple. Ferrocene was used as internal standard. Spectroelectrochemical measurements were performed in an optically transparent thin-layer electrochemical cell²⁶ with minigrad platinum working and auxiliary electrodes and silver microwire pseudoreference electrode. The cell was connected to a computer-controlled PAR Model 283 potentiostat. UV-vis spectra were recorded with a Hewlett-Packard HP 8453 diode-array spectrophotometer.

Experimental X-band EPR spectra were recorded on a Bruker EMX spectrometer. The spectra were simulated by iteration of the anisotropic *g* values, (super)hyperfine coupling constants, and line widths using the W9SEPR program (available upon request from Prof. Frank Neese, Max Planck Institute for Bioinorganic Chemistry).

Flash chromatography: silica gel SiliaFlash P60 (0.040–0.063 mm) with an overpressure of about 0.5 bar. Melting points were measured on samples in unsealed capillaries on a Stuart Scientific SMP3 melting point apparatus and are uncorrected. (*Z*)-1,2-Bis(2-bromophenyl)ethene (**5**)²⁷ and mesityldichlorophosphine²⁸ were prepared according to the literature procedures.

DFT Calculations. DFT Conformational Analysis. The conformational analysis of [6a] and [6b]^{•-}, as well as the spin state energies of [6a]²⁻, were evaluated with Gaussian03 at the B3PW91 level of theory. In this functional, the exchange energy is described with contributions from local and nonlocal (B3-parameter Becke²⁹ and Hartree–Fock (HF)) exchange terms, and the correlation energy is given by the Perdew and Wang 91³⁰ nonlocal functional within the generalized gradient approximation (GGA).³¹ The 6-311G(d,p) basis set for atoms C, H, N, O, and P has been used. The nature of each stationary point was confirmed by a frequency calculation. Relative energies were corrected with zero-point energies.

DFT Property Calculations. The geometries of the full atom models of [6a], [6a]^{•-}, [6a]²⁻, [6b]^{•-}, and [6b]²⁻ were optimized with the Turbomole program^{21a} coupled to the PQS Baker optimizer³² at the BP86 DFT level³³ using the Turbomole SV(P) basis.^{21c,f} The EPR parameters³⁴ of [6a]^{•-} and [6b]^{•-} were subsequently calculated with ORCA,¹⁹ using the B3LYP³³ functional and TZVP^{21c,f} basis set supplied with the program (Ahlich polarization functions on all atoms). The calculations were performed according to the spin unrestricted coupled-perturbed Kohn–Sham formalism, which expresses the *g* tensor as a second-order response property with respect to homogeneous external magnetic field and spin–orbit coupling (SOC) perturbations.³⁵ Calculation of the hyperfine interactions takes the SOC effects into account.³⁶ The UV-vis parameters of [6a]^{•-} and [6a]²⁻ were calculated with ORCA at the TD-DFT b3-lyp, def2-TZVP level employing COSMO³⁷ dielectric solvent corrections ($\epsilon = 2.28$). The coordinates from the structure optimized in Turbomole were used as inputs for the ORCA calculations. Orbital and spin density plots were generated with Molden.³⁸

Synthetic Procedures. 5-Phenyl-5H-dibenzo[*b,f*]phosphepine–Borane (7a). A solution of (*Z*)-1,2-bis(2-bromophenyl)ethene (**5**;²⁷ 1.83 mmol, 618 mg) in 9 mL of diethyl ether was added dropwise to a solution of *t*-BuLi (7.32 mmol, 4.58 mL of 1.6 M solution in pentane) in 9 mL of diethyl ether at –78 °C, and the mixture was stirred for 1 h at this temperature. Then, phenyldichlorophosphine (1.83 mmol, 328 mg, 0.25 mL) was added, and the reaction mixture was warmed to room temperature. After the mixture was stirred at room temperature for 1.5 h, a 2.0 M solution of BH₃–SMe₂ in diethyl ether (1.92 mmol, 0.96 mL) was added dropwise, and the resulting mixture was stirred overnight followed by the addition of water (10 mL) and diethyl ether (20 mL), filtration through Celite, and column chromatography purification on silica (Et₂O/pentane 1/1). This gave 448 mg (1.49 mmol, 82% yield) of **7a** as a colorless solid. It is recommended to monitor the reaction by ³¹P NMR before isolation, since in some cases we observed slow formation of the BH₃ adduct (this, probably, depends on the quality of BH₃–SMe₂). If conversion is not completed, more BH₃–SMe₂ solution should be added. Mp: 182–184 °C (colorless crystals). ¹H NMR (400 MHz, CDCl₃): 1.35 (q, 3H, ¹J_{HB} = 78.8 Hz, BH₃), 6.81 (s, 2H, *H*-1), 6.90–6.92 (m, 2H, *o*-Ph), 7.18 (td, 2H, ²J_{HH} = 7.9, ⁴J_{HP} = 2.3 Hz, *m*-Ph), 7.30 (m, 1H, *p*-Ph), 7.46–7.49 (m, 2H, *H*-2), 7.59–7.64 (m, 4H, *H*-3, *H*-5), 8.42–8.47 (m, 2H, *H*-4). ³¹P{¹H} NMR (162 MHz, CDCl₃): 13.4 (q, ¹J_{PB} = 71.8 Hz). ¹¹B NMR (128 MHz, CDCl₃): –37.9 (m). ¹³C{¹H} NMR (101 MHz, CDCl₃): 126.8 (d, ¹J_{CP} = 55.8 Hz, *C*-5a), 128.0 (d, ³J_{CP} = 10.6 Hz, *m*-Ph), 128.9 (d, ²J_{CP} = 12.6 Hz, *C*-5), 129.6 (d, ¹J_{CP} = 61.5 Hz, *i*-Ph), 130.1 (d, ⁴J_{CP} = 2.6 Hz, *p*-Ph), 130.2 (d, ³J_{CP} = 6.5 Hz, *C*-2), 130.9 (d, ²J_{CP} = 10.1 Hz, *o*-Ph), 131.7 (d, ⁴J_{CP} = 1.8 Hz, *C*-2), 132.5 (d, ³J_{CP} = 1.4 Hz, *C*-10), 135.1 (d, ³J_{CP} = 17.8 Hz, *C*-4), 139.3 (*C*-1a). IR: $\tilde{\nu}$ 3058 (w), 3016 (w), 2379 (s), 2343 (m), 1476 (m), 1437 (m), 1140 (m), 1062

(s), 807 (s), 733 (s), 697 (s), 616 (m), 460 (s). HR-FAB MS: calcd for $C_{20}H_{17}BP$ ($M - H$) 299.1165, found 299.1169; m/z (%) 299 (100) [$M - H$], 209 (15) [$M - BH_3 - Ph$], 178 (25) [$M - BH_3 - Ph - P$], 154 (80), 136 (60), 107 (20) [C_6H_4P].

5-Phenyl-5H-dibenzo[*b,f*]phosphepine (6a). A 1.14 g portion (10.2 mmol) of DABCO was added to a solution of 1.53 g (5.1 mmol) of **7a** in 40 mL of toluene at room temperature, and the mixture was stirred overnight. The next day the mixture was quenched with a 5% aqueous solution of HCl and extracted with diethyl ether. The combined organic extracts were dried with $MgSO_4$, and all volatiles were removed under reduced pressure. This gave 1.42 g (4.97 mmol, 97%) of phosphine **6a** as a colorless solid. It is recommended to monitor the reaction by ^{31}P NMR before isolation, since in some cases we observed slow deborylation of the BH_3 adduct. If conversion is not completed, more DABCO should be added. Mp: 132–134 °C (colorless solid). 1H NMR (500 MHz, $CDCl_3$): 6.78 (s, 2H, *H-1*), 6.90 (dd, 2H, $^2J_{HH} = 7.7$, $^4J_{HP} = 1.7$ Hz, *m-Ph*), 7.13–7.20 (m, 3H, *o*-, *p-Ph*), 7.39–7.46 (m, 6H, *H-2*, *H-3*, *H-4/S*), 7.83–7.88 (m, 2H, *H-5/4*). $^{31}P\{^1H\}$ NMR (162 MHz, $CDCl_3$): -8.1. $^{13}C\{^1H\}$ NMR (126 MHz, $CDCl_3$): 127.4 (*p-Ph*), 127.7 (d, $^2J_{CP} = 4.8$ Hz, *o-Ph*), 128.2 (d, $J_{CP} = 15.2$, *C-4/S*), 129.7 (d, $^4J_{CP} = 0.7$ Hz, *C-3*), 130.5 (d, $^3J_{CP} = 1.6$ Hz, *C-2*), 131.4 (d, $^3J_{CP} = 16.3$ Hz, *m-Ph*), 132.6 (d, $^3J_{CP} = 1.3$ Hz, *C-1*), 135.8 (d, $^1J_{CP} = 9.3$ Hz, *C-5a*), 137.0 (d, $J_{CP} = 45.8$ Hz, *C-5/4*), 137.4 (d, $^1J_{CP} = 9.5$ Hz, *i-Ph*), 139.9 (*C-1a*). IR: $\tilde{\nu}$ 3048 (m), 3009 (m), 1476 (m), 1427 (m), 1264 (m), 804 (s), 775 (s), 740 (s), 694 (s), 496 (m), 460 (s). HR-ESI MS: calcd for $C_{20}H_{16}P$ ($M + H$) 287.0984, found 297.0979; m/z (%) 287 (100) [$M + H$], 219 (10), 165 (80).

Reduction of 6a with Sodium. Compound **6a** (143 mg, 0.5 mmol) was dissolved in 1.5 mL of THF, and 115 mg (5.0 mmol) of sodium was added to this solution at room temperature. Upon stirring, the reaction mixture changed color from reddish to deep purple. After 4 h of stirring at room temperature the solution was decanted from unreacted sodium. The mixture was ^{31}P NMR silent. Crystals of the dianionic species [**6a**] $^{2-}$ were obtained by slow evaporation of pentane into the THF solution obtained after decantation from sodium; these were also ^{31}P NMR silent.

5-Mesityl-5H-dibenzo[*b,f*]phosphepine–Borane (7b). A solution of (*Z*)-1,2-bis(2-bromophenyl)ethene (**5**; 27 4.70 mmol, 1.59 g) in 30 mL of diethyl ether was added dropwise to a solution of *t*-BuLi (18.82 mmol, 11.7 mL of a 1.7 M solution in pentane) in 30 mL of diethyl ether at -78 °C, and the mixture was stirred for 1 h at this temperature. Then, mesityldichlorophosphine 28 (mixture of $MesPCl_2$ and $MesPClBr$, approximately 4/1, 4.70 mmol, 1.08 g) in 15 mL of diethyl ether was added, and the reaction mixture was warmed to room temperature. The mixture was stirred at room temperature overnight. Full conversion was observed with ^{31}P NMR. After that a 2.0 M solution of BH_3-SMe_2 in diethyl ether (4.94 mmol, 2.47 mL) was added dropwise to the reaction mixture at room temperature. The mixture was stirred overnight, followed by the addition of water (20 mL) and diethyl ether (40 mL), filtration through Celite, and column chromatography purification on silica (MTBE/pentane 10/0.1, then 10/1). This gave 520 mg (1.52 mmol, 32% yield) of **7b** as a colorless solid. It is recommended to monitor the reaction by ^{31}P NMR before isolation, since in some cases we observed slow formation of the BH_3 adduct (this, probably, depends on the quality of BH_3-SMe_2). If conversion is not completed, more BH_3-SMe_2 solution should be added. Mp: 181–183 °C (colorless crystals). 1H NMR (400 MHz, $CDCl_3$): 1.43 (q, 3H, $^1J_{HB} = 79.5$ Hz, BH_3), 1.55 (s, 6H, *o-CH_3*(Mes)), 2.19 (s, 3H, *p-CH_3*(Mes)), 6.63 (d, 2H, $^4J_{HP} = 2.8$ Hz, *m-Mes*), 6.85 (s, 2H, *H-1*), 7.38 (d, 2H, $^4J_{HP} = 6.9$ Hz, *H-2*), 7.48–7.57 (m, 4H, *H-3*, *H-4*), 8.36–8.42 (m, 2H, *H-5*). $^{31}P\{^1H\}$ NMR (162 MHz, $CDCl_3$): 10.4 (q, $^1J_{PB} = 74.1$ Hz). ^{11}B NMR (128 MHz, $CDCl_3$): -39.8 (m). $^{13}C\{^1H\}$ NMR (101 MHz, $CDCl_3$): 20.9 (s, *p-CH_3*(Mes)), 22.8 (d, $^3J_{CP} = 5.5$ Hz, *o-CH_3*(Mes)), 121.5 (d, $^1J_{CP} = 57.2$ Hz, *i-Mes*), 128.7 (d, $^3J_{CP} = 6.6$ Hz, *C-2*), 129.2 (d, $^3J_{CP} = 13.0$ Hz, *C-4*), 130.5 (d, $^1J_{CP} = 56.1$ Hz, *C-5a*), 130.68 (*C-3*), 130.73 (d, $^3J_{CP} = 6.5$ Hz, *m-Mes*), 131.7 (d, $^3J_{CP} = 1.7$ Hz, *C-1*), 133.1 (d, $^2J_{CP} = 18.1$ Hz, *C-5*), 138.4 (*C-1a*), 139.7 (d, $^4J_{CP} = 2.6$ Hz, *p-Mes*), 142.0 (d, $^2J_{CP} = 8.5$ Hz, *o-Mes*). IR: $\tilde{\nu}$ 3058 (w), 3016 (w), 2970 (w), 2927 (w), 2382 (s), 2343 (m), 1451 (m), 1136 (w), 1058 (s), 804 (s), 775 (m), 743 (m), 460 (m). HR-

FAB MS: calcd for $C_{23}H_{23}BP$ ($M - H$) 341.1635, found 341.1639; m/z (%) 341 (100) [$M - H$], 328 (55) [$M - BH_3$], 209 (20) [$M - BH_3 - Mes$], 183 (20) [$M - BH_3 - Mes - CH=CH$], 150 (15).

5-Mesityl-5H-dibenzo[*b,f*]phosphepine (6b). A 1.47 g portion (13.10 mmol) of DABCO was added to a solution of 447 mg (1.31 mmol) of **7b** in 20 mL of dichloromethane at room temperature, and the mixture was stirred overnight. The next day the mixture was filtered over a silica pad and then through Celite, washed with a 5% aqueous solution of HCl, and extracted with diethyl ether. The combined organic extracts were dried with $MgSO_4$, and all volatiles were evaporated under reduced pressure. This gave 398 mg (1.31 mmol, 96%) of phosphine **6b** as a yellowish solid. It is recommended to monitor the reaction by ^{31}P NMR before isolation, since in some cases we observed slow deborylation of the BH_3 adduct. If conversion is not completed, more DABCO should be added. Mp: 183–186 °C (yellowish solid). 1H NMR (400 MHz, $CDCl_3$): 2.42 (s, 6H, *o-CH_3*(Mes)), 2.43 (s, 3H, *p-CH_3*(Mes)), 6.81 (t, 2H, $J_{HH} = 6.8$ Hz), 6.96 (s, 2H, *H-1*), 7.10–7.14 (m, 4H), 7.17–7.24 (m, 4H). $^{31}P\{^1H\}$ NMR (162 MHz, $CDCl_3$): -30.5. $^{13}C\{^1H\}$ NMR (101 MHz): 21.4 (*p-CH_3*(Mes)), 24.6 (d, $^2J_{CP} = 18.9$ Hz, *o-CH_3*(Mes)), 125.5 (d, $^3J_{CP} = 8.4$ Hz), 127.4, 128.5, 129.7 (d, $J_{CP} = 6.3$ Hz), 129.8 (d, $J_{CP} = 4.7$ Hz), 130.4 (d, $J_{CP} = 4.7$ Hz), 134.7 (d, $^3J_{CP} = 6.3$ Hz, *C-1*), 137.8 (d, $J_{CP} = 16.5$ Hz), 138.6 (d, $J_{CP} = 21.0$ Hz), 140.6 (d, $J_{CP} = 1.4$ Hz), 147.0 (d, $J_{CP} = 17.2$). IR: $\tilde{\nu}$ 3051 (w), 3012 (w), 2963 (w), 2917 (w), 2853 (w), 1469 (m), 1423 (m), 1094 (m), 1027 (m), 800 (s), 747 (s). HR-FAB MS: calcd for $C_{23}H_{22}P$ ($M + H$) 329.1459, found 329.1459; m/z (%) 328 (60) [M], 281 (20), 207 (25), 147 (40), 73 (100).

Reduction of 5-Mesityl-5H-dibenzo[*b,f*]phosphepine (6b) with Sodium. Reduction was carried out similarly to the reduction of the phosphepine **6a**. The mixture was ^{31}P NMR silent.

Tris(5-phenyl-5H-dibenzo[*b,f*]phosphepine)rhodium(I) Triflate (8a[OTf]). A solution of dibenzophosphepine **6a** (0.34 mmol, 97 mg) in 5 mL of dichloromethane was added to a solution of dicyclooctadiene rhodium(I) triflate (0.11 mmol, 51 mg) in 5 mL of dichloromethane at room temperature. The mixture was stirred for 6 h, all volatiles were removed by vacuum evaporation, and the solid was washed with pentane in order to get rid of COD. This gave **8a** as a yellow solid in quantitative yield. Crystals suitable for an X-ray study can be obtained by dissolution of the complex in DCM and slow evaporation of pentane into this solution. Mp: >270 °C (dec without melting). 1H NMR (500 MHz, CD_2Cl_2 , 215 K): 4.31 (s, $CH=CH$), 4.85 (s, $CH=CH$), 5.41–5.64 (m, *Ar*), 6.06 (s, $CH=CH$), 6.58–7.91 (m, *Ar*). $^{31}P\{^1H\}$ NMR (202 MHz, CD_2Cl_2 , 215 K): 19.7 (ddd, $^1J_{PRh} = 119.0$, $^2J_{PP} = 38.1$, $^2J_{PP} = 21.8$ Hz, 1P), 31.4 (ddd, $^2J_{PP} = 395.0$, $^1J_{PRh} = 95.2$, $^2J_{PP} = 21.8$ Hz, 1P), 39.2 (ddd, $^2J_{PP} = 395.0$, $^1J_{PRh} = 95.2$, $^2J_{PP} = 38.1$ Hz, 1P). $^{19}F\{^1H\}$ NMR (235 MHz, CD_2Cl_2 , 298 K): -153.7. IR: $\tilde{\nu}$ 2966 (w), 2920 (w), 2850 (w), 1455 (w), 1356 (w), 1278 (m), 1260 (s), 1083 (m), 1027 (s), 793 (s). HR-FAB MS: calcd for $C_{60}H_{45}P_3Rh$ ($M - OTf$) 961.1789, found 961.1786; m/z (%) 961 (12) [$M - OTf$], 675 (100) [$M - OTf - 6a$], 497 (10), 389 (25) [$M - OTf - 26a$], 154 (48), 136 (33).

Bis(5-mesityl-5H-dibenzo[*b,f*]phosphepine)rhodium(I) Triflate (8b[OTf]). A solution of dibenzophosphepine **6b** (0.30 mmol, 100 mg) in 2 mL of dichloromethane was added at room temperature to a solution of dicyclooctadiene rhodium(I) triflate (0.15 mmol, 71 mg) in 2 mL of dichloromethane. The mixture was stirred at room temperature for 2 h, and then all volatiles were removed by vacuum evaporation and the solid was washed with diethyl ether. This gave 130 mg (0.14 mmol, 93%) of a mixture of *cis* and *trans* isomers of complex **8b** (the ratio according to ^{31}P NMR is 1/0.1). The major isomer can be obtained by slow crystallization from a dichloromethane solution of the mixture, covered by pentane. This gives 75 mg (0.083 mmol, 55%) of the *cis* isomer as deep red needles. $^{31}P\{^1H\}$ NMR of the crude mixture of *cis* and *trans* isomers (signal ratio is 1/0.1; 101 MHz, CD_2Cl_2): 34.6 (d, $^1J_{PRh} = 149.0$ Hz), 43.1 (d, $^1J_{PRh} = 127.3$ Hz). Mp 243–246 °C (red solid). NMR spectra of the purified *cis-8b*[OTf]: 1H NMR (400 MHz, CD_2Cl_2) 1.97 (s, 6H, *o-CH_3*(Mes)), 2.32 (s, 3H, *p-CH_3*(Mes)), 6.20 (s, 2H, *H-1*), 6.70 (s, 2H, *m-Mes*), 7.09–7.14 (m, 2H, *H-3/4/5*), 7.21–7.26 (m, 4H, *H-3/4/5*), 7.51 (d, 2H, $J = 4.6$ Hz, *H-2*); $^{31}P\{^1H\}$ NMR (162 MHz, CD_2Cl_2) 34.6 (d, $^1J_{PRh} = 149.0$ Hz);

$^{19}\text{F}\{^1\text{H}\}$ NMR (235 MHz, CD_2Cl_2) -78.7 ; $^{13}\text{C}\{^1\text{H}\}$ NMR (101 MHz, CD_2Cl_2) 21.2 (*p*- $\text{CH}_3(\text{Mes})$), 27.3 (*o*- $\text{CH}_3(\text{Mes})$), 96.6 (C-1), 113.9 (d, $^1J_{\text{CP}} = 44.1$ Hz, *i*-Mes), 121.5 (q, $^1J_{\text{CF}} = 318.8$ Hz, CF_3), 127.1 (C-3/4/5), 127.5 (t, $^3J_{\text{CP}} \approx ^3J_{\text{CRh}} = 7.0$ Hz, C-2), 129.6 (C-3/4/5), 129.9 (C-3/4/5), 131.4 (t, $^3J_{\text{CP}} \approx ^4J_{\text{CRh}} = 3.9$ Hz, *m*-Mes), 134.9 (d, $J_{\text{CP}} = 43.1$ Hz, C-5a/1a), 142.0 (*p*-Mes), 142.5 (*o*-Mes), 144.2 (d, $J_{\text{CP}} = 22.6$ Hz, C-1a/5a). IR: $\tilde{\nu}$ 3058 (w), 2966 (w), 2920 (w), 1455 (m), 1260 (s), 1154 (m), 1030 (s), 779 (m), 637 (s). HR-FAB MS: calcd for $\text{C}_{46}\text{H}_{42}\text{P}_2\text{Rh}$ (M - OTf) 759.1817, found 759.1809; m/z (%) 759 (100) [M - OTf], 431 (50) [M - OTf - **6b**], 311 (12), 154 (37), 136 (30).

Bis(5-mesityl-5H-dibenzo[b,f]phosphepine)rhodium(II) Tetrakis-[3,5-(trifluoromethyl)phenyl]borate (8b[BARf]). OTf \rightarrow BARf exchange was achieved according to the procedure of Grützmacher et al.^{6a} Complex **8b** (X = OTf; 265 mg, 0.292 mmol) and NaBARf (269 mg, 0.304 mmol) were stirred in 10 mL of DCM (dry) overnight. A white precipitate (NaOTf) was filtered off over Celite. The solvent was removed under reduced pressure, and the red solid was dissolved in 3 mL of diethyl ether, layered with 10 mL of hexane, and crystallized overnight. The product was filtered off and dried under reduced pressure, which gave 376 mg (0.223 mmol, 80%) of **8b** (X = BARf) as a deep red crystalline product. The complex is air stable and soluble in DCM, THF, and diethyl ether. Mp: 205–210 °C dec (red solid). ^1H NMR (400 MHz, CD_2Cl_2): 2.00 (s, 12H, *o*- $\text{CH}_3(\text{Mes})$), 2.35 (s, 6H, *p*- $\text{CH}_3(\text{Mes})$), 6.03 (s, 4H), 6.74 (s, 4H), 7.15–7.20 (m, 4H), 7.25–7.32 (m, 8H), 7.45–7.49 (m, 4H), 7.60 (s, 4H), 7.77 (s, 8H). $^{31}\text{P}\{^1\text{H}\}$ NMR (162 MHz, CD_2Cl_2): 33.3 (d, $^1J_{\text{PRh}} = 142.8$ Hz). ^{11}B NMR (128 MHz, CDCl_3): -6.6 (s). $^{19}\text{F}\{^1\text{H}\}$ NMR (235 MHz, CD_2Cl_2): -62.8 . $^{13}\text{C}\{^1\text{H}\}$ NMR (126 MHz, CD_2Cl_2): 20.7 (*p*- $\text{CH}_3(\text{Mes})$), 26.9 (*o*- $\text{CH}_3(\text{Mes})$), 95.7, 113.0, 117.4, 124.6 (q, $^1J_{\text{CF}} = 278.4$ Hz, CF_3), 126.8, 126.9, 128.9 (q, $^2J_{\text{CF}} = 30.8$ Hz, C- CF_3), 129.3, 129.8, 131.1, 134.4, 134.8, 141.9, 142.2, 143.4 (d, $J = 20.3$ Hz), 161.8 (q, $^1J_{\text{CB}} = 49.7$ Hz, C-B). IR: $\tilde{\nu}$ 3072 (w), 2927 (w), 1610 (w), 1455 (w), 1352 (m), 1278 (s), 1126 (s), 881 (w). HR-FAB MS: calcd for $\text{C}_{46}\text{H}_{42}\text{P}_2\text{Rh}$ (M - BARf) 759.1817, found 759.1828; m/z (%) 759 (100) [M - OTf], 431 (50) [M - BARf - **6b**], 310 (12), 251 (6), 178 (4).

■ ASSOCIATED CONTENT

Supporting Information

Text, figures, tables, and CIF files giving experimental synthetic procedures, Cartesian coordinates and energies of all stationary points (DFT), crystallographic data, NMR spectra of all new compounds, EPR spectra of the compounds [**6a** $^{\bullet-}$] and [**6b** $^{\bullet-}$], and cyclic voltammograms of **6a**, **8a**, and **8b**. This material is available free of charge via the Internet at <http://pubs.acs.org>.

■ AUTHOR INFORMATION

Corresponding Author

*E-mail: B.deBruin@uva.nl (B.d.B.); k.lammertsma@vu.nl (K.L.).

Notes

The authors declare no competing financial interest.

■ ACKNOWLEDGMENTS

The work was financially supported by the Council for Chemical Sciences of The Netherlands Organization for Scientific Research (NWO/CW), the European Research Council (Grant Agreement 202886), the University of Amsterdam, and the VU University Amsterdam.

■ REFERENCES

(1) For some recent reviews, see: (a) Cucciolito, M. E.; De Felice, V.; Roviello, G.; Ruffo, F. *Eur. J. Inorg. Chem.* **2011**, 457–469. (b) Canovese, L.; Visentin, F. *Inorg. Chim. Acta* **2010**, 363, 2375–2386. (c) Wang, X.-S.; Zhao, H.; Li, Y.-H.; Xiong, R.-G.; You, X.-Z. *Top. Catal.* **2005**, 35, 43–61. (d) Kurosawa, H.; Ikeda, I. *J. Organomet.*

Chem. **1992**, 428, 289–301. (e) Weding, N.; Hapke, M. *Chem. Soc. Rev.* **2011**, 40, 4525–4538.

(2) Reviews: (a) Herndon, J. W. *Coord. Chem. Rev.* **2010**, 254, 103–194. (b) de Bruin, B.; Hettterscheid, D. J. H. *Eur. J. Inorg. Chem.* **2007**, 211–230. (c) Adams, R. D. *Chem. Soc. Rev.* **1994**, 335–339. (d) Hahn, C. *Chem. Eur. J.* **2004**, 10, 5888–5899.

(3) (a) Maire, P.; Deblon, S.; Breher, B.; Geier, J.; Böhler, C.; Rügger, H.; Schönberg, H.; Grützmacher, H. *Chem. Eur. J.* **2004**, 10, 4198–4205. (b) Piras, E.; Läng, F.; Rügger, H.; Stein, D.; Wörle, M.; Grützmacher, H. *Chem. Eur. J.* **2006**, 12, 5849–5858. (c) Ferrer, C.; Benet-Buchholz, J.; Riera, A.; Verdaguer, X. *Chem. Eur. J.* **2010**, 16, 8340–8346. (d) Hayashi, T.; Ueyama, K.; Tokunaga, N.; Yoshida, K. *J. Am. Chem. Soc.* **2003**, 125, 11508–11509. (e) Fischer, C.; Defieber, C.; Suzuki, T.; Carreira, E. M. *J. Am. Chem. Soc.* **2004**, 126, 1628–1629. (f) Puschmann, F. F.; Grützmacher, H.; de Bruin, B. *J. Am. Chem. Soc.* **2010**, 132, 73–75. (g) Böhler, C.; Avarvari, N.; Schönberg, H.; Wörle, M.; Rügger, H.; Grützmacher, H. *Helv. Chim. Acta* **2001**, 84, 3127–3147. (h) Thoumazet, C.; Grützmacher, H.; Deschamps, B.; Ricard, L.; le Floch, P. *Eur. J. Inorg. Chem.* **2006**, 3911–3922. (i) Narui, R.; Hayashi, S.; Otomo, H.; Shintani, R.; Hayashi, T. *Tetrahedron: Asymmetry* **2012**, 23, 284–293. (j) Bernard, M.; Guiral, V.; Delbecq, F.; Fache, F.; Sautel, P.; Lemaire, M. *J. Am. Chem. Soc.* **1998**, 120, 1441–1446.

(4) For a review on the use of chiral olefins and related chiral hetero bidentate amine–olefin and phosphane–olefin ligands in asymmetric catalysis, see: Defieber, C.; Grützmacher, H.; Carreira, E. M. *Angew. Chem., Int. Ed.* **2008**, 47, 4482–4502.

(5) Pregosin, P. S. *Chem. Commun.* **2008**, 4875–4884.

(6) (a) Puschmann, F. F.; Harmer, J.; Stein, D.; Rügger, H.; de Bruin, B.; Grützmacher, H. *Angew. Chem., Int. Ed.* **2010**, 49, 385–389. (b) Puschmann, F. F.; Grützmacher, H.; de Bruin, B. *J. Am. Chem. Soc.* **2010**, 132, 73–75.

(7) Piras, E.; Läng, F.; Rügger, H.; Stein, D.; Wörle, M.; Grützmacher, H. *Chem. Eur. J.* **2006**, 12, 5649–5858.

(8) Campos, J.; López-Serrano, J.; Álvarez, E.; Carmona, E. *J. Am. Chem. Soc.* **2012**, 134, 7165–7175.

(9) (a) Lyaskovskyy, V.; Elders, N.; Ehlers, A. W.; Lutz, M.; Slootweg, J. C.; Lammertsma, K. *J. Am. Chem. Soc.* **2011**, 133, 9704–9707. (b) Jansen, H.; Samuels, M. C.; Couzijn, E. P. A.; Slootweg, J. C.; Ehlers, A. W.; Chen, P.; Lammertsma, K. *Chem. Eur. J.* **2010**, 16, 1454–1458. (c) Borst, M. L. G.; Bulo, R. E.; Winkel, C. W.; Gibney, D. J.; Ehlers, A. W.; Schakel, M.; Lutz, M.; Spek, A. L.; Lammertsma, K. *J. Am. Chem. Soc.* **2005**, 127, 5800–5801.

(10) Märkl, G.; Burger, W. *Angew. Chem., Int. Ed. Engl.* **1984**, 23, 894–895.

(11) (a) Jansen, H.; Slootweg, J. C.; Ehlers, A. W.; Lammertsma, K. *Organometallics* **2010**, 29, 6653–6659. (b) Yasuike, S.; Kiharada, T.; Kurita, J.; Tsuchiya, T. *Chem. Commun.* **1996**, 2183–2184. (c) Kassae, M. Z.; Cheshmehkani, A.; Musavi, S. M.; Majdi, M.; Motamedi, E. *J. Mol. Struct. (THEOCHEM)* **2008**, 865, 73–78.

(12) (a) Märkl, G.; Burger, W. *Tetrahedron Lett.* **1983**, 24, 2545–2548. (b) Yasuike, S.; Kiharada, T.; Tsuchiya, T.; Kurita, J. *Chem. Pharm. Bull.* **2003**, 51, 1283–1288. (c) Kurita, J.; Shiratori, S.; Yasuike, S.; Tsuchiya, T. *J. Chem. Soc., Chem. Commun.* **1991**, 1227–1228.

(13) Yasuike, S.; Ohta, H.; Shiratori, S.; Kurita, J.; Tsuchiya, T. *J. Chem. Soc., Chem. Commun.* **1993**, 1817–1819.

(14) Alternatively, dibenzophosphepines can be first converted to the corresponding phosphane oxides, followed by purification and subsequent reduction to the phosphanes with silanes: Segall, Y.; Shirin, E.; Granoth, I. *Phosphorus, Sulfur, Silicon Relat. Elem.* **1980**, 8, 243–254. A direct isolation (without the phosphorus protection step) of the phosphepine **6a** has also been reported,¹³ but the latter procedure did not work in our hands.

(15) Dunne, B. J.; Orpen, A. J. *Acta Crystallogr.* **1991**, C47, 345–347.

(16) Frisch, M. J.; Trucks, G. W.; Schlegel, H. B.; Scuseria, G. E.; Robb, M. A.; Cheeseman, J. R.; Montgomery, J. A., Jr.; Vreven, T.; Kudin, K. N.; Burant, J. C.; Millam, J. M.; Iyengar, S. S.; Tomasi, J.; Barone, V.; Mennucci, B.; Cossi, M.; Scalmani, G.; Rega, N.; Petersson, G. A.; Nakatsuji, H.; Hada, M.; Ehara, M.; Toyota, K.;

- Fukuda, R.; Hasegawa, J.; Ishida, M.; Nakajima, T.; Honda, Y.; Kitao, O.; Nakai, H.; Klene, M.; Li, X.; Knox, J. E.; Hratchian, H. P.; Cross, J. B.; Bakken, V.; Adamo, C.; Jaramillo, J.; Gomperts, R.; Stratmann, R. E.; Yazyev, O.; Austin, A. J.; Cammi, R.; Pomelli, C.; Ochterski, J. W.; Ayala, P. Y.; Morokuma, K.; Voth, G. A.; Salvador, P.; Dannenberg, J. J.; Zakrzewski, V. G.; Dapprich, S.; Daniels, A. D.; Strain, M. C.; Farkas, O.; Malick, D. K.; Rabuck, A. D.; Raghavachari, K.; Foresman, J. B.; Ortiz, J. V.; Cui, Q.; Baboul, A. G.; Clifford, S.; Cioslowski, J.; Stefanov, B. B.; Liu, G.; Liashenko, A.; Piskorz, P.; Komaromi, I.; Martin, R. L.; Fox, D. J.; Keith, T.; Al-Laham, M. A.; Peng, C. Y.; Nanayakkara, A.; Challacombe, M.; Gill, P. M. W.; Johnson, B.; Chen, W.; Wong, M. W.; Gonzalez, C.; Pople, J. A. *Gaussian 03, Revision C.02*; Gaussian, Inc., Wallingford, CT, 2004.
- (17) (a) Hettterscheid, D. G. H.; Kaiser, J.; Reijerse, E.; Peters, T. P. J.; Thewissen, S.; Blok, A. N. J.; Smits, J. M. M.; de Gelder, R.; de Bruin, B. *J. Am. Chem. Soc.* **2005**, *127*, 1895–1905. (b) de Bruin, B.; Peters, T. P. J.; Thewissen, S.; Blok, A. N. J.; Wilting, J. B. M.; de Gelder, R.; Smits, J. M. M.; Gal, A. W. *Angew. Chem., Int. Ed.* **2002**, *41*, 2135–2138. (c) Hettterscheid, D. G. H.; Bens, M.; de Bruin, B. *Dalton Trans.* **2005**, *5*, 979–984. (d) Review: de Bruin, B.; Hettterscheid, D. G. H. *Eur. J. Inorg. Chem.* **2007**, *2*, 211–230. (e) Review: Hettterscheid, D. G. H.; Grütmacher, H.; Koekoek, A. J. J.; de Bruin, B. *Prog. Inorg. Chem.* **2007**, *55*, 247–253.
- (18) (a) Lyaskovskyy, V.; de Bruin, B. *ACS Catal.* **2012**, *2*, 270–279. (b) Forum Issue on Redox Non-Innocent Ligands: *Inorg. Chem.*, **2011**, *50*, 9737. (c) Special issue on “Cooperative & Redox Non-Innocent Ligands in Directing Organometallic Reactivity”: *Eur. J. Inorg. Chem.* **2012**, *3*, 340. (d) Kaim, W.; Schwederski, B. *Coord. Chem. Rev.* **2010**, *254*, 1580–1588. (e) Chirik, P. J.; Wieghardt, K. *Science* **2010**, *327*, 794–795.
- (19) Neese, F. *ORCA-an ab initio, Density Functional and Semi-empirical program package, Version 2.9*; Max-Planck-Institut für Bioanorganische Chemie, Mülheim an der Ruhr, Germany, 2009.
- (20) Connelly, N. G.; Geiger, W. E. *Chem. Rev.* **1996**, *96*, 877–910.
- (21) (a) Ahlrichs, R.; Bär, M.; Baron, H.-P.; Bauernschmitt, R.; Böcker, S.; Ehrig, M.; Eichkorn, K.; Elliott, S.; Furche, F.; Haase, F.; Häser, M.; Hättig, C.; Horn, H.; Huber, C.; Huniar, U.; Kattannek, M.; Köhn, A.; Kölmel, C.; Kollwitz, M.; May, K.; Ochsenfeld, C.; Öhm, H.; Schäfer, A.; Schneider, U.; Treutler, O.; Tsereteli, K.; Unterreiner, B.; von Arnim, M.; Weigend, F.; Weis, P.; Weiss, H. *Turbomole Version 5, January 2002*; Theoretical Chemistry Group, University of Karlsruhe, Karlsruhe, Germany, 2002. (b) Treutler, O.; Ahlrichs, R. *J. Chem. Phys.* **1995**, *102*, 346–354. (c) Turbomole basis set library, Turbomole Version 5; see ref 21a. (d) Schäfer, A.; Horn, H.; Ahlrichs, R. *J. Chem. Phys.* **1992**, *97*, 2571–2577. (e) Andrae, D.; Haeussermann, U.; Dolg, M.; Stoll, H.; Preuss, H. *Theor. Chim. Acta* **1990**, *77*, 123–141. (f) Schäfer, A.; Huber, C.; Ahlrichs, R. *J. Chem. Phys.* **1994**, *100*, 5829–5835.
- (22) Addison, A. W.; Rao, T. N.; Reedijk, J.; van Rijn, J.; Verschoor, G. C. *Dalton Trans.* **1984**, 1349–1356.
- (23) Calculated from the simplified Eyring equation $\Delta G^\ddagger = (4.575 \times 10^{-3})T_c[9.972 + \log(T_c/\Delta\nu)]$ (kcal mol⁻¹), where T_c is the coalescence temperature (in K; $T_c = 298$ K for **8a**) and $\Delta\nu$ is the difference in chemical shifts (Hz) at 215 K.
- (24) de Bruin, B.; Russcher, J. C.; Grütmacher, H. *J. Organomet. Chem.* **2007**, *692*, 3167–3173 and references therein.
- (25) For the disproportionation equilibrium $2[\mathbf{8b}^\bullet]^- \rightleftharpoons [\mathbf{8b}]^{2-} + \mathbf{8b}$, $\Delta G^\circ = 33.8$ kJ mol⁻¹ and $K_{\text{disp}} \approx 1 \times 10^{-7}$.
- (26) Krejčík, M.; Daněš, M.; Hartl, F. *J. Electroanal. Chem.* **1991**, *317*, 179–187.
- (27) Dunne, E. C.; Coyne, É. J.; Crowley, P. B.; Gilheany, D. G. *Tetrahedron Lett.* **2002**, *43*, 2449–2453.
- (28) Nief, F.; Mathey, F. *Tetrahedron* **1991**, *47*, 6673–6680.
- (29) Becke, A. D. *J. Chem. Phys.* **1993**, *98*, 5648–5652.
- (30) (a) Perdew, J. P.; Chevary, J. A.; Vosko, S. H.; Jackson, K. A.; Pederson, M. R.; Singh, D. J.; Fiolhais, C. *Phys. Rev. B* **1992**, *46*, 6671–6687. (b) Perdew, J. P.; Wang, Y. *Phys. Rev. B* **1992**, *45*, 13244–13249. (c) Perdew, J. P. Unified Theory of Exchange and Correlation Beyond the Local Density Approximation. In *Electronic Structure of Solids*; Ziesche, P.; Eschrig, H., Eds.; Akademie Verlag: Berlin, 1991; Vol. 11. (d) Perdew, J. P.; Chevary, J. A.; Vosko, S. H.; Jackson, K. A.; Pederson, M. R.; Singh, D. J.; Fiolhais, C. *Phys. Rev. B* **1992**, *46*, 6671–6687. (e) Perdew, J. P.; Burke, K.; Wang, Y. *Phys. Rev. B* **1996**, *54*, 16533–16539. (f) Burke, K.; Perdew, J. P.; Wang, Y. Derivation of a Generalized Gradient Approximation: The PW91 Density Functional. In *Electronic Density Functional Theory and New Directions*; Dobson, J. F., Vignale, G., Das, M. P., Eds.; Plenum: New York, 1998; Vol. 81.
- (31) Jensen, F. *Introduction to Computational Chemistry*, 3rd ed.; Wiley: Chichester, U.K., 1999; p 429.
- (32) (a) PQS version 2.4; Parallel Quantum Solutions, Fayetteville, AK, 2001 (the Baker optimizer is available separately from PQS upon request). (b) Baker, J. J. *Comput. Chem.* **1986**, *7*, 385–395.
- (33) (a) Lee, C.; Yang, W.; Parr, R. G. *Phys. Rev. B* **1988**, *37*, 785–789. (b) Becke, A. D. *J. Chem. Phys.* **1993**, *98*, 1372–1377. (c) Becke, A. D. *J. Chem. Phys.* **1993**, *98*, 5648–5652.
- (34) Some references and reviews on DFT approaches to EPR parameters: (a) van Lenthe, E.; van der Avoird, A.; Wormer, P. E. S. *J. Chem. Phys.* **1997**, *107*, 2488–2498. (b) van Lenthe, E.; van der Avoird, A.; Wormer, P. E. S. *J. Chem. Phys.* **1998**, *108*, 4783–4796. (c) Neese, F. *Curr. Opin. Chem. Biol.* **2003**, *7*, 125–135. (d) Neese, F.; Solomon, E. In *Magnetoscience-From Molecules to Materials*; Miller, J. S., Drillon, M., Eds.; Wiley: New York, 2003; pp 345–466. (e) Peng, G.; Nichols, J.; McCullough, E. A.; Spence, J. *Inorg. Chem.* **1994**, *33*, 2857–2864.
- (35) Neese, F. *J. Chem. Phys.* **2001**, *115*, 11080–11096.
- (36) Neese, F. *J. Chem. Phys.* **2003**, *118*, 3939–3948.
- (37) Klamt, A.; Schüürmann, G. *J. Chem. Soc., Perkin Trans. 2* **1993**, 799–805.
- (38) Schaftenaar, G.; Noordik, J. H. *J. Comput.-Aided Mol. Des.* **2000**, *14*, 123–134.